Journal of Colloid and Interface Science 543 (2019) 43–51

Contents lists available at ScienceDirect

Journal of Colloid and Interface Science

journal homepage: www.elsevier.com/locate/jcis

Regular Article

# Efficient removal of methylene blue from aqueous solutions using magnetic graphene oxide modified zeolite

Tiantian Huang [a,1], Ming Yan [a,1], Kai He [a,1], Zhenzhen Huang [a,1], Guangming Zeng [a,*], Anwei Chen [b,*], Min Peng [a], Hui Li [a], Lei Yuan [a], Guiqiu Chen [a]

[a] College of Environmental Science and Engineering, Hunan University and Key Laboratory of Environmental Biology and Pollution Control (Hunan University), Ministry of Education, Changsha 410082, PR China
[b] College of Resources and Environment, Hunan Agricultural University, Changsha 410128, PR China

## GRAPHICAL ABSTRACT

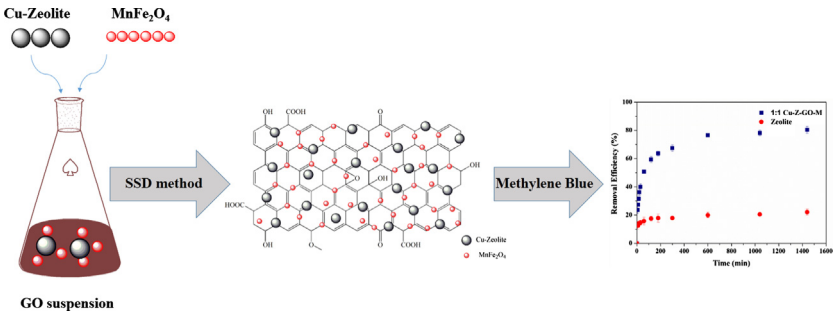


## ARTICLE INFO

*Article history:*
Received 20 November 2018
Revised 6 February 2019
Accepted 7 February 2019
Available online 10 February 2019

*Keywords:*
Zeolite
Graphene oxide
$MnFe_2O_4$
Methylene blue
Adsorption

## ABSTRACT

In this study, magnetic graphene oxide modified zeolite (Cu-Z-GO-M) composites with two different ratios of GO to zeolite (named Cu-Z-GO-M 1:2 and Cu-Z-GO-M 1:1) were synthesized by solid-state dispersion (SSD) method. The properties of zeolite-based composites were characterized by SEM, XRD, FTIR, XPS, and magnetization curves. In order to understand the pollutant removal performance of the as-prepared composites, methylene blue (MB) was used as the target pollutant in adsorption experiments. The removal efficiency of MB onto Cu-Z-GO-M composite was enhanced obviously with pH > 9. The adsorption capacities of MB onto Cu-Z-GO-M 1:1 were 82.147, 89.315, 97.346 mg/g at 298, 308, and 318 K, respectively. The removal ability of MB increased with the increase of GO content in modified composites. The adsorption behavior can be well described using a pseudo-second-order kinetic and Freundlich isotherm model. The thermodynamic analysis indicated the MB adsorption by Cu-Z-GO-M was a spontaneous and endothermic reaction. The results showed that the prepared Cu-Z-GO-M composite could be a promising adsorbent with good adsorption capacity and reusability for MB removal from wastewater.



## 1. Introduction

Dyes effluent discharged from textile, paper-making, printing, food additives, leather, cosmetic and other industries have caused serious environmental pollution [1,2]. Nowadays, dye pollution has

* Corresponding authors.
*E-mail addresses:* zgming@hnu.edu.cn (G. Zeng), A.Chen@hunau.edu.cn (A. Chen).
[1] These authors contribute equally to this article.

https://doi.org/10.1016/j.jcis.2019.02.030
0021-9797/

attracted great attention over the world, due to its toxicity to human being as well as the fauna and flora even at a low concentration [3]. The toxic effects of dyes effluent on human being will cause allergy, cutitis, skin stimulus, and even cancer [4,5]. Therefore, the waste water containing dyes must be treated before discharging into the natural water bodies. Various approaches including precipitation [6], ion exchange [7], photocatalytic degradation [8,9], biological oxidation [10,11], adsorption [12,13], membrane filtration [14] and electrochemical function have been applied to remove dyes from wastewater. Among these methods, adsorption has been regarded as a most commonly used method for water purification, because of its low cost, easy operation and flexibility [15].

Zeolite, a common mineral absorbent with adequate deposits, low cost, and organophilic cations [16], has been widely used for dye adsorption from wastewater. For example, the natural zeolite has been reported in many investigations for dye removal [17–19]. However, the lower adsorption capacity of natural zeolite limits its widely application as an absorbent. In order to improve its adsorption performance, various modified zeolite composites have been fabricated. Jin et al. [18] reported that the adsorption capacity of SDBS-modified zeolite was twice larger than that of original zeolite towards anionic orange II. Erol Alver et al. [20] also reported that the adsorption capacities of anionic dyes (reactive red 239 and reactive blue 250) onto zeolite with hexamethylenediamine modification were up to 28.57 and 17.63 mg/g at 293 K, respectively. Although, these reports showed that modified zeolites had higher adsorption capacity as compared to that of the unmodified zeolite, those modification approaches still could not obtain a satisfactory adsorption performance. Therefore, seeking an appropriate modification method to functionalize zeolite and improve its performance is still required.

Graphene oxide (GO), a typical product of graphene, has a particular structure of a two-dimensional (2D) honeycomb lattice with a single layer of $sp^2$ carbon atoms [21–23]. To date, GO has been applied as an efficient adsorbent for pollutant removal owing to its unique structure and physicochemical properties, such as a large surface area, abundant oxygen-containing functional groups [24,25] and excellent physicochemical abilities [26,27]. However, it is difficult to separate GO from aqueous solution due to its excellent hydrophilicity. Therefore, the design of solid hybrid GO-based materials is a good method to improve its application in pollutants removal. Importantly, the pollutant removal performance of raw materials could be enhanced after its modification [28,29]. To our knowledge, the research on the application of GO modified zeolite composite for cationic dye removal is limited. Thus, it is worth to explore the dye removal by GO modified zeolite composite. In order to make the synthesis of hybrid successfully, $Cu^{2+}$ ions were used as a coordination cation to bond zeolite to GO sheets [30]. Nevertheless, composites modified by GO are difficult to collect after reaction. Magnetic separation technology has been widely applied for the solid-liquid separation. Herein, $MnFe_2O_4$ with short synthesis time, high crystallinity and low cost was introduced onto Cu-Zeolite/GO composites to make it possible to reuse the materials [31], which can be conveniently separated by an external magnet.

In this study, magnetic Cu-Zeolite/GO composites were fabricated using a facile method. In order to investigate their pollutant removal performance, methylene blue (MB), a typical cationic dye was selected as a model pollutant for adsorption experiments. A series of experiments were carried out to determine the influence of various factors such as pH, time, and temperature on dyes adsorption by magnetic Cu-Zeolite/GO composite.

## 2. Experimental

### 2.1. Materials

GO was prepared according to the modified Hummer method [32,33]. Artificial zeolite ($Na_2O{\cdot}Al_2O_3{\cdot}xSiO_2{\cdot}yH_2O$) was obtained from Sinopharm chemical Reagent Co., Ltd., Ethanol, $CuSO_4{\cdot}5H_2O$, $FeCl_3{\cdot}6H_2O$, $MnSO_4{\cdot}H_2O$, MB, and all other chemicals used were analytical reagent grade and purchased from Sinopharm chemical Reagent Co., Ltd without further purification. Deionized water was used in all experiments.

### 2.2. Synthesis of composites

#### 2.2.1. Synthesis of $MnFe_2O_4$ nanoparticles

Magnetic nanoparticles were synthesized by the coprecipitation method [34–37]. Briefly, 2.703 g of $FeCl_3{\cdot}6H_2O$ and 0.845 g of $MnSO_4{\cdot}H_2O$ were dissolved in 100 mL of deionized water under stirring to get a molar ratio of Mn:Fe in the solution at 1:2. Then, solution pH was slowly adjusted to 10 using 8 M NaOH until the solution turned orange into black brown, followed by continuous stirring for another 30 min. After the homogeneous dispersion was placed at 90 °C in water bath for 2 h, the black precipitates were magnetically separated by a magnet and washed with deionized water for several times to remove the unreacted part. Finally, the precipitates ($MnFe_2O_4$) were dried at 60 °C overnight.

#### 2.2.2. Synthesis of Cu-Z-GO-M composites

To prepare the Cu-Zeolite, 1 g of zeolite was added into 100 mL of $CuSO_4{\cdot}5H_2O$ solution (0.02 M), followed by magnetic stirring for 24 h [36]. Whereafter, the suspension was washed with 0.01 M sulfuric acid and deionized water to remove residues. Ultimately, Cu-Zeolite was dried in air and ground into powder for further use.

The preparation of Cu-Z-GO-M was conducted by SSD method [38]. Different amounts of GO were added into ethanol followed by ultrasonication treatment for 3 h. Then, 0.125 g of as-prepared Cu-Zeolite and 0.8 g of magnetic particles $MnFe_2O_4$ were added into the homogeneous distributed suspension to get the mixture of two different mass ratios of GO to Cu-zeolite (w/w, 1:1 and 1:2). Subsequently, the above-mentioned mixtures were stirred by the muddler until the solvent of the solution was all evaporated. Finally, the achieved blackish precipitate was dried at 60 °C.

### 2.3. Characterization

The surface morphology of zeolite-based samples was investigated by Field Emission Scanning Electron Microscope (FE-SEM, JSM-6700F, Japan). The X-ray photoelectron spectroscopy (XPS) was used to characterize the elemental compositions and the surface functional groups of the zeolite samples, which was performed on ESCALAB 250Xi (Thermo Fisher Scientific, USA). The surface chemical properties of the samples were characterized by attenuated total reflection-Fourier transform infrared spectroscopy (ATR-FTIR, NICOLET 5700 FT-IR Spectrometer, USA), which was recorded between 400 and 4000 $cm^{-1}$. The structure and crystallinity of samples were recorded on an X-ray diffractometer (XRD) (D/max-2500, Rigaku, Japan) in a 2θ range of 4–70°. The specific surface area (SSA) was recorded on Brunauer-Emmett-Teller (BET) method and the nitrogen was used as absorbent. Magnetic properties of the samples were characterized on a vibrating sample magnetometer (VSM, Mpms (squid) XL-7, Quantum, USA) at 25 °C.

### 2.4. Adsorption tests

In this work, MB, one of the most common cationic dyes, was used as a target pollutant to study the adsorption performance of

Cu-Z-GO-M composites. A series of adsorption experiments were carried out by appending a certain amount of absorbent (10 mg) into 30 mL MB solution in a shaker (160 r/min) at room temperature (25 °C). The influence of initial MB concentration on the adsorption was carried out with MB concentration ranging from 20 to 70 mg/L. Herein, initial dye concentration at 40 mg/L was applied to investigate adsorption in other influenced conditions. The effect of solution pH on the MB removal was carried out from pH 4.0 to 10.0. The adsorption thermodynamic was investigated at different temperatures (25, 35, and 45 °C). Different concentrations of NaCl solutions (0.01, 0.05, 0.1, 0.2, and 0.5 M) were employed to examine the effect of ionic strength on the dye removal. After adsorption, Cu-Z-GO-M composites were separated using an external magnet. The initial and residual concentrations of MB were measured by a UV spectrophotometer (Pgeneral T6, Beijing, China) at 664 nm. The removal efficiency R (%) and the amount of MB adsorbed $q_e$ (mg/g) at equilibrium per unit mass of samples were calculated with the following equations:

$$R = \frac{C_0 - C_e}{C_0} \times 100\% \quad (1)$$

$$Q_e = \frac{(C_0 - C_e)}{m} \times V \quad (2)$$

where $C_0$ (mg/L) and $C_e$ (mg/L) are the initial and the equilibrium concentrations of MB, respectively. $V$ (L) stands for the volume of MB solution, and $m$ (g) represents the mass of samples added into the MB solution.

## 3. Results and discussion.

### 3.1. Characterizations of samples

The morphology of raw zeolite, GO and Cu-Z-GO-M samples was observed by SEM micrograph (Fig. 1). As shown in Fig. 1a, the crystal surface of zeolite is obvious. The typical properties of GO image, such as the smooth surface, the wrinkled ripples and a thinner layer are also observed (Fig. 1b) [39]. Additionally, Cu-Zeolite is more densely distributed on GO sheets in Fig. 1c comparing with that in Fig. 1d. The rough morphology of Cu-Z-GO-M sample (1:1) could provide more adsorption sites owing to a larger surface area.

The XRD patterns of GO, raw zeolite, $MnFe_2O_4$ and Cu-Z-GO-M composites are displayed in Fig. 2a. The characteristic peak at $2\theta = 10.8°$ is corresponding to GO, manifesting abundant existence of oxygen function groups on the GO layers [40]. $MnFe_2O_4$ and Cu-Z-GO-M composites exhibited similar XRD patterns in Fig. 2a. The standard peaks of $MnFe_2O_4$ at the $2\theta = 30.04°$, 35.50°, 42.98°, 53.32°, 56.74° and 62.56° are all presented on these three XRD patterns, as mentioned above [41]. The weak peaks at $2\theta = 7.19°$, 10.19°, 12.54°, 21.39°, 27.64°, 30.19° and 35.59° are related to zeolite [38], which are presented in the XRD patterns of Cu-Z-GO-M samples. There are no significant peaks of GO sheets in Cu-Z-GO-M composites, which might attribute to the strong signals of $MnFe_2O_4$ flow the relatively weak carbon peaks. These results indicated the preparation of the Cu-Z-GO-M composites was successful.

As shown in Fig. 2b, the magnetization hysteresis curves of Cu-Z-GO-M samples at room temperature display a typical shape like a letter "S". The zero retentivity and coercivity in Fig. 2b demonstrate the super magnetization of the Cu-Z-GO-M [42]. The saturations magnetization of Cu-Z-GO-M (1:1) and Cu-Z-GO-M (1:2) are 0.02829 and 0.01478 emu/mg, respectively, which indicates the ferromagnetic properties and the success of solid-liquid separation by an external magnet. Furthermore, the separation behavior is displayed in the inset of Fig. 2b, which indicates that the Cu-Z-GO-M samples could be separated from the reaction system by a magnet. Hence, the magnetization property of Cu-Z-GO-M samples made it easier to collect from the reaction solution to save the cost.

As shown in Fig. 3a, the FTIR spectra of samples are tested in the range of 4000–400 $cm^{-1}$. The FTIR spectra show characteristic peaks (449, 602, 704, and 1027 $cm^{-1}$) in the curve of Cu-Z-GO-M composites which relate to $TO_4$ (T=Si and Al) of zeolite. Several typical peaks of GO, such as C—O—C (1053 $cm^{-1}$), C=O (1730 $cm^{-1}$), and O—H (3408 $cm^{-1}$) are also observed in the spectra of Cu-Z-GO-M samples, indicating that the Cu-Z-GO-M samples were successfully synthesized by GO. Additionally, the characteristic peak of Fe—O at 580 $cm^{-1}$ comes from the magnetic material of $MnFe_2O_4$. Therefore, the analysis mentioned above proved the Cu-Z-GO-M samples were synthesized successfully by SSD method.

The XPS spectra of zeolite and Cu-Z-GO-M (1:1 and 1:2) samples are represented in Fig. 3b. The XPS survey spectrum of raw zeolite shows five elements peaks, containing Al, Si, C, O, and Na, locating at 80.72, 108.7, 284.6, 533.0 and 1072.2 eV, respectively. The full scan spectra of Cu-Z-GO-M samples show the peaks at binding energies of 642 and 711.4 eV which correspond to Mn 2p and Fe 2p species respectively. To further determine the chemical composition and main functional groups, the C1s XPS spectra of 1:2 Cu-Z-GO-M (Fig. 3c) and 1:1 Cu-Z-GO-M (Fig. 3d) were carried out. Three peaks center at the binding energy of about 284.6, 286.2, and 286.9 eV are observed from Fig. 3d, corresponding to C=C/C—C, C—O, and C—O—C, respectively [43].

Additionally, the element analysis of zeolite and Cu-Z-GO-M samples based on XPS spectra is listed in Table 1. With the introduction of GO and $MnFe_2O_4$, the content of carbon atom raised from 13.97% to 34.80% and 36.78%, the content of Na reduced from 11.54% to 0.29% and 0.11%, and the content of Si and Al were both decreased. The variations of element ratio in these three samples manifested that the successful modification of its surface properties. Furthermore, the surface area of zeolite samples increased (from 25.566 to 46.696 $m^2/g$) with the increasing content of GO adding to zeolite samples. The higher surface area might provide more adsorption sites which are beneficial for the removal of MB. The analysis results of XPS indicate that the Cu-Z-GO-M samples are successfully prepared by the method in this study. These results were compliant with the XRD and FTIR characteristics.

### 3.2. Adsorption tests

#### 3.2.1. Effect of pH

The variations in the removal efficiency of MB at different solution pH are shown in Fig. 4. The solution pH could not only influence the degree of deprotonation and the formation of surface functional groups of the absorbent, but also affect the species of the MB [44]. As shown in Fig. 4, with the increase of solution pH, the removal efficiency of MB onto Cu-Z-GO-M (1:1) was higher than two other composites. The removal efficiency of MB by Cu-Z-GO-M (1:1) absorbent was still at the maximum (64.09%) as the pH value was 4.0, whereas the removal efficiencies of Cu-Z-GO-M (1:2) and zeolite were 38.27% and 16.86%, respectively, which might due to that the addition of the large amount of GO to zeolite could offer more adsorption sites and powerful interaction of adsorption (π–π interactions) [28]. When pH < 8.0, the removal efficiencies toward MB of three composites showed no remarkable change. However, the removal efficiency of MB onto Cu-Z-GO-M composites were significantly enhanced at pH > 8.0 as compared with that of zeolite because the high concentration of $H_3O^+$ under acid condition led to great competitive with MB for adsorption sites, further attributing to the relatively low MB removal.

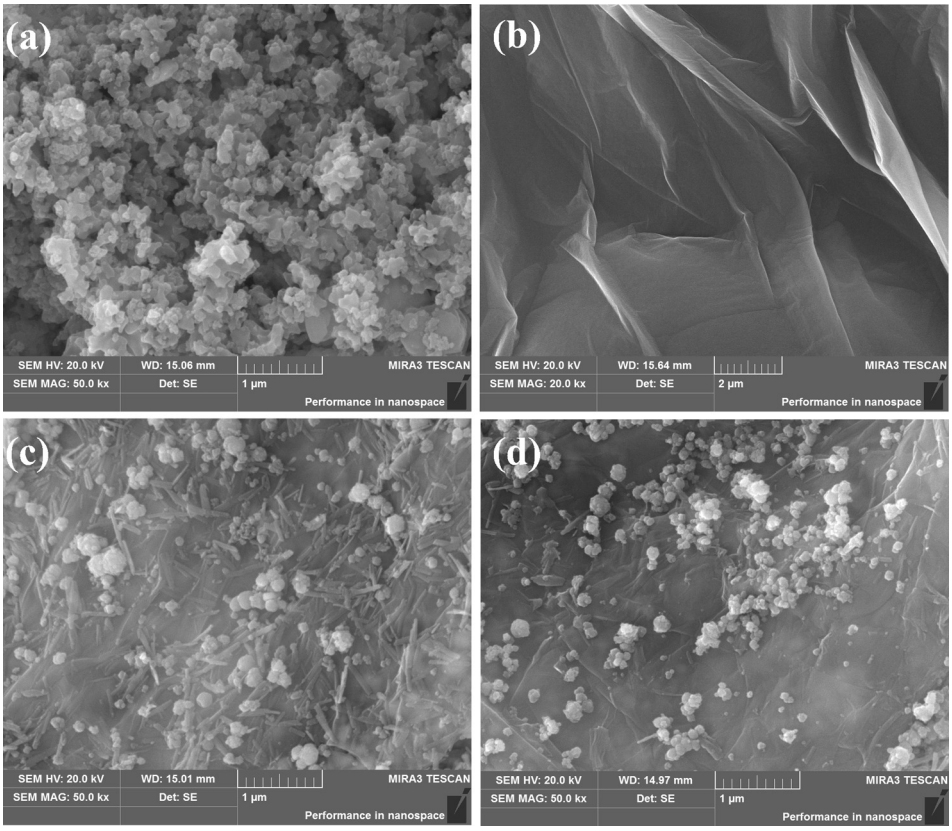


**Fig. 1.** SEM images of raw zeolite (a), GO (b), Cu-Z-GO-M (1:2) (c) and Cu-Z-GO-M (1:1) (d).

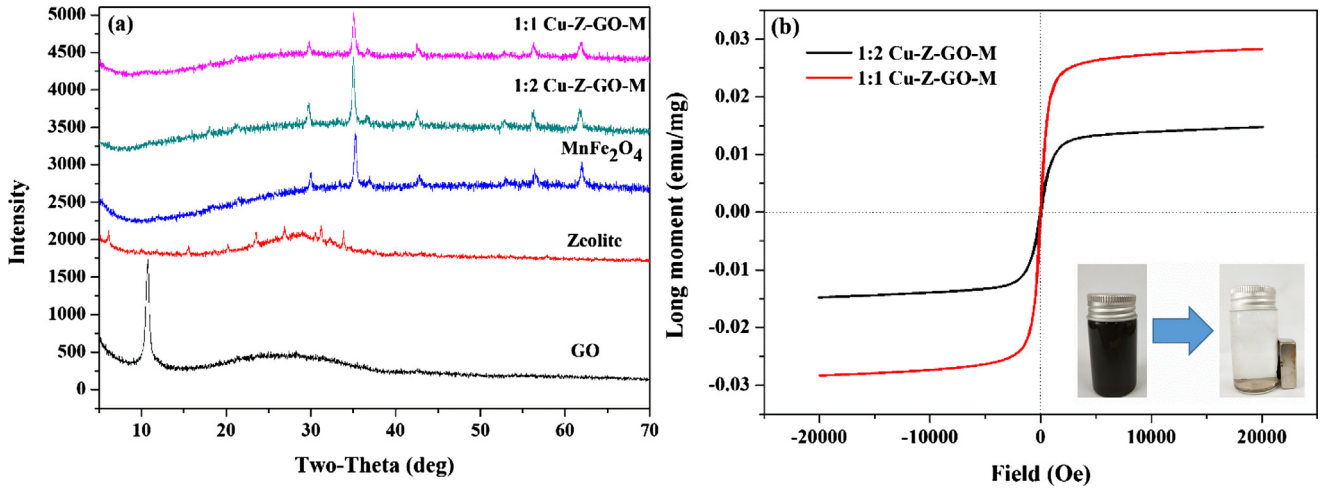


**Fig. 2.** XRD patterns (a) of GO, Zeolite, $MnFe_2O_4$, Cu-Z-GO-M (1:2) and Cu-Z-GO-M (1:1); Magnetization curves (b) of Cu-Z-GO-M (1:2) and Cu-Z-GO-M (1:1) at room temperature.

*3.2.2. Effect of contact time and adsorption kinetics*

The effect of contact time on the removal efficiency of MB was investigated with the contact time from 0 to 24 h. It is obvious that the removal rate of MB by Cu-Z-GO-M samples is very rapid and the adsorption reaches equilibrium within 10 h (Fig. 5a). Furthermore, the absorption capacities are 27.486, 59.148, and 99.162 mg/g for zeolite, Cu-Z-GO-M (1:2), and Cu-Z-GO-M (1:1), respectively (Fig. 5b). Significantly, the adsorption quantity of decorated zeolite was much larger than that of undecorated zeolite. The absorption capacity of Cu-Z-GO-M (1:1) for MB was approximately 1.7 times larger than that of Cu-Z-GO-M (1:2), which was attributed to a larger amount of oxygen-containing functional groups on the surface of the Cu-Z-GO-M (1:1).

In order to figure out the adsorption mechanism of zeolite composites, the experimental data was fitted with two frequently-used kinetic models (pseudo-first-order and pseudo-second order) [45,46]. The detailed equations of the kinetic models above-mentioned are described as follows:

Pseudo-first-order kinetic model

$$q_t = q_{e,1}\left(1 - e^{-k_1 t}\right) \tag{3}$$

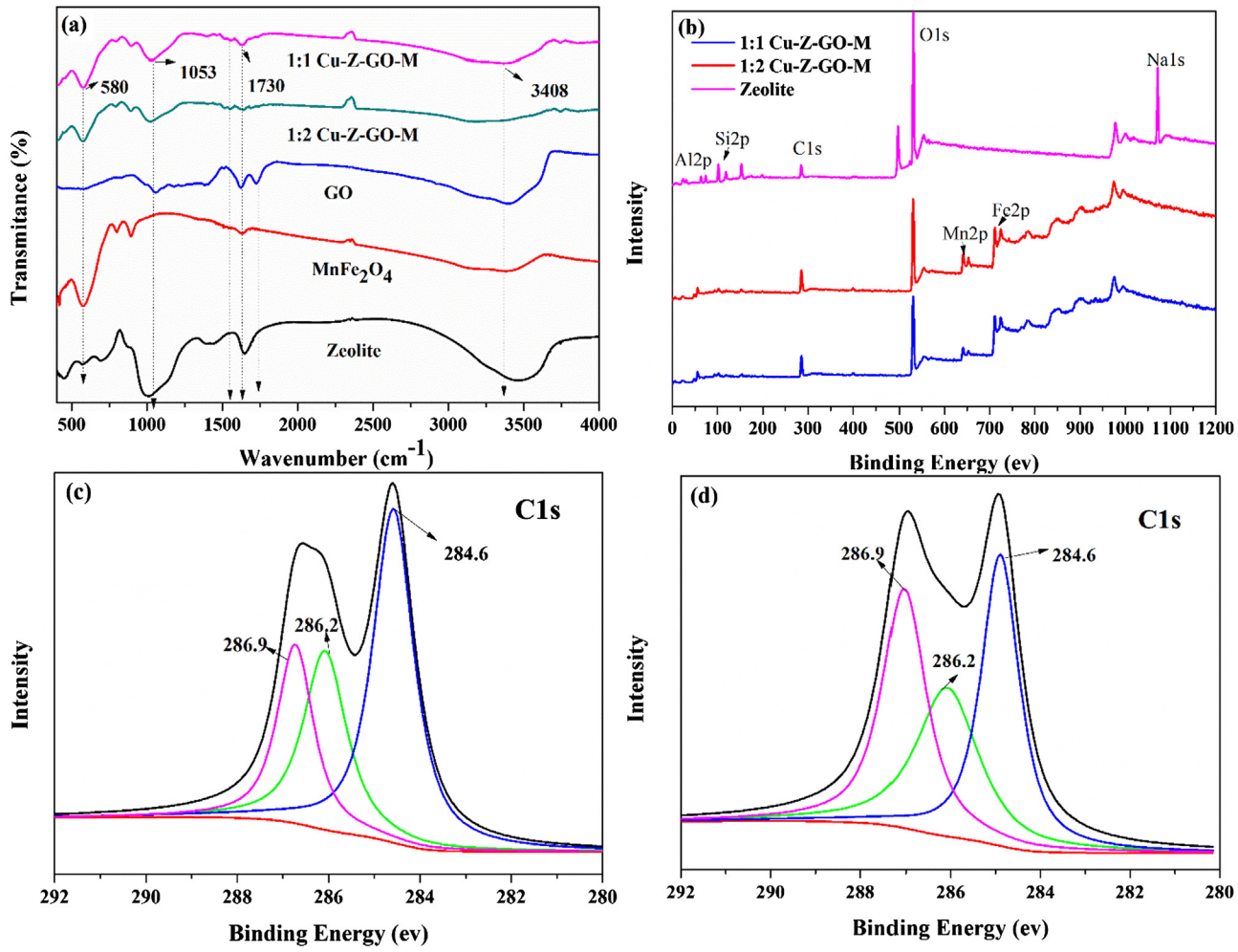


**Fig. 3.** FTIR spectra (a) of zeolite, GO, $MnFe_2O_4$, and Cu-Z-GO-M samples (1:2 and 1:1); XPS full scans (b) of zeolite and GO-Z-GO-M samples; C1s XPS spectra of (c) Cu-Z-GO-M (1:2) and (d) Cu-Z-GO-M (1:1).

**Table 1**
Element composition, atom ratios, and BET-$N_2$ surface area (SA) of adsorbents.

| Samples | Atom percentage | | | | | SA ($m^2$/g) |
|---|---|---|---|---|---|---|
| | C1s | O1s | Si2p | Al2p | Na1s | |
| Zeolite | 13.97 | 52 | 13.93 | 8.55 | 11.54 | 25.566 |
| 1:2 Cu-Z-GO-M | 34.80 | 51.49 | 6.46 | 6.96 | 0.29 | 43.068 |
| 1:1 Cu-Z-GO-M | 36.78 | 52.02 | 5.42 | 5.67 | 0.11 | 46.696 |

Pseudo-second-order kinetic model

$$q_t = \frac{q_{e,2}^2 k_2 t}{1 + k_2 q_{e,2} t} \quad (4)$$

where $q_t$ (mg/g) is the amount of absorbed MB onto the absorbent at different time (min), $q_{e,1}$ and $q_{e,2}$ are the mass of the adsorption quantity of MB onto absorbents by non-linear pseudo-first-order and non-linear pseudo-second-order models, respectively, and $k_1$ ($min^{-1}$) and $k_2$ (g/mg min) are the rate constants of the pseudo-first-order and the pseudo-second-order models, respectively.

After being fitted by the two kinetic models displayed in Fig. 5b, the calculated parameters for the MB onto zeolite composites are listed in Table 2. It is clearly seen from Table 2 that the adsorption of MB onto the three absorbents is better described by the pseudo-second order model according to the value of correlation coefficient ($R^2$). From this result, it follows that the adsorption process of MB onto the absorbents proceeded by chemisorption mechanism [47].

*3.2.3. Effect of temperature and adsorption isotherm*

A series of experiments with initial concentrations of MB onto Cu-Z-GO-M (1:1) were executed to figure out the adsorption behavior between solid and liquid phase as the adsorption reached saturation [48]. Fig. 6 displays that a higher temperature is more beneficial to the adsorption of MB onto Cu-Z-GO-M (1:1). In this study, the two common adsorption isotherm models, the Langmuir and Freundlich models, were used to investigate the interaction of molecules and surface of adsorbent by the data at adsorption equilibrium. The slow adsorption rate might be due to the reduction of the active sites on the surface of Cu-Z-GO-M (1:1) [49].

Langmuir adsorption isotherm model

The Langmuir isotherm is on the basis of the assumption that adsorption sites on the surface of the adsorbent are restricted and distributed homogeneously. The adsorbate is absorbed without mutual interaction and has the same attraction for adsorption. It is represented by the equation as below:

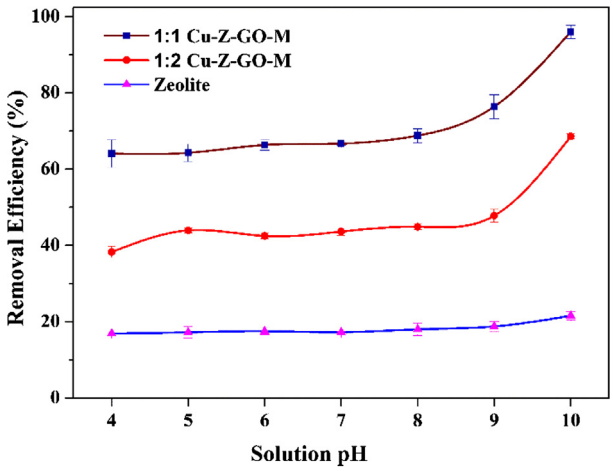


**Fig. 4.** Effect of solution pH on the removal efficiency of MB onto absorbents.

$$q_e = \frac{q_{maxK_LC_e}}{1 + K_L C_e} \tag{5}$$

where $q_e$ (mg/g) and $C_e$ (mg/L) represent quantity and the concentration of adsorption respectively, and $q_{max}$ (mg/g) is the theoretic adsorption quantity at equilibrium. $K_L$ (L/mg) is Langmuir isotherm constant which reflects the power of adsorption experiments.

Freundlich adsorption isotherm model

The Freundlich isotherm model is used to give a description of the adsorption behavior that occurs on the heterogeneous surface [50]. The well-known expression for Freundlich isotherm model is presented in the following form:

$$q_e = K_F C_e^{\frac{1}{n}} \tag{6}$$

where $q_e$ (mg/g) and $C_e$ (mg/L) are on the behalf of the adsorption quantity and concentration of MB towards Cu-Z-GO-M (1:1) at the equilibrium, respectively. $K_F$ [(mg/g)(L/mg)$^{1/n}$] is Freundlich isotherm constant. The value of n in the equation is another constant in Freundlich isotherm model to indicate how favorable the adsorption process. If $0 < 1/n < 1$, the adsorption process is in favor of the reaction condition; if $1/n > 1$, it is un-favorable; if $1/n = 1$, manifesting the process is homogeneous [51].

Adsorption parameters are presented in Table 3. It is significant that the correlation coefficient ($R^2$) of Freundlich isotherm model is much higher than that of Langmuir isotherm model, which indicates that the Freundlich model describes the adsorption process better. Furthermore, the adsorption of MB adsorption is heterogeneous and multilayer [52]. Otherwise, Table 2 displays that the $q_{max}$ of MB onto Cu-Z-GO-M (1:1) in the Langmuir model is enhanced with increasing temperature, which might be due to the fact that the interaction between MB and the active sites were reinforced in the enhancement of temperature. Compared with other reported absorbents displayed in Table 4, Cu-Z-GO-M (1:1) exhibits approving adsorption performance towards MB. Therefore, the zeolite modified by a certain content of GO could enhance the adsorption capacity of MB.

To further evaluate the influence of adsorption factors on MB adsorption process by Cu-Z-GO-M (1:1), the effect of temperature on adsorption process was investigated. As shown in Fig. 6, three different temperatures (298, 308, and 318 K) were set to expand the adsorption experiments of MB onto Cu-Z-GO-M (1:1). Significantly, the higher temperature could improve the removal ability of MB by Cu-Z-GO-M (1:1), which might be explained by the enhanced interaction between the active sites and MB molecules at higher temperature. Commonly, the thermodynamic parameters, such as Gibbs free energy ($\Delta G^0$), entropy ($\Delta S^0$), and enthalpy ($\Delta H$), were calculated from the following equations [55]:

$$\ln K_d = \frac{\Delta S^0}{R} - \frac{\Delta H^0}{RT} \tag{7}$$

$$\Delta G^0 = \Delta H^0 - T\Delta S^0 \tag{8}$$

where $K_d$ is produced by $q_e/C_e$. T (K) is the absolute temperature in Kelvin, $\Delta S$ [KJ (K$^{-1}$·mol$^{-1}$)] is the entropy change, $\Delta H$ (KJ/mol) is the enthalpy constant, and $R$ is the universal gas constant [8.314 KJ/(mol·K)]. The values of $\Delta S$ and $\Delta H$ are determined from the slope and intercept of the Van't Hoff plots of $\ln K_d$ versus of 1/T in Fig. 6.

Table 5 presents the detailed values of the thermodynamic parameters. The values of $\Delta G$ decrease from −2.789 to −3.509 with the temperature increasing from 298 to 318 K, manifesting that the adsorption of MB onto absorbent in this study is spontaneous [56]. Additionally, the value of $\Delta H$ is positive, indicating the reaction is endothermic [57]. Furthermore, the positive value of $\Delta S$ elucidates the randomness on the surface of solid/solution, showing an increasing trend during the attachment process [58].

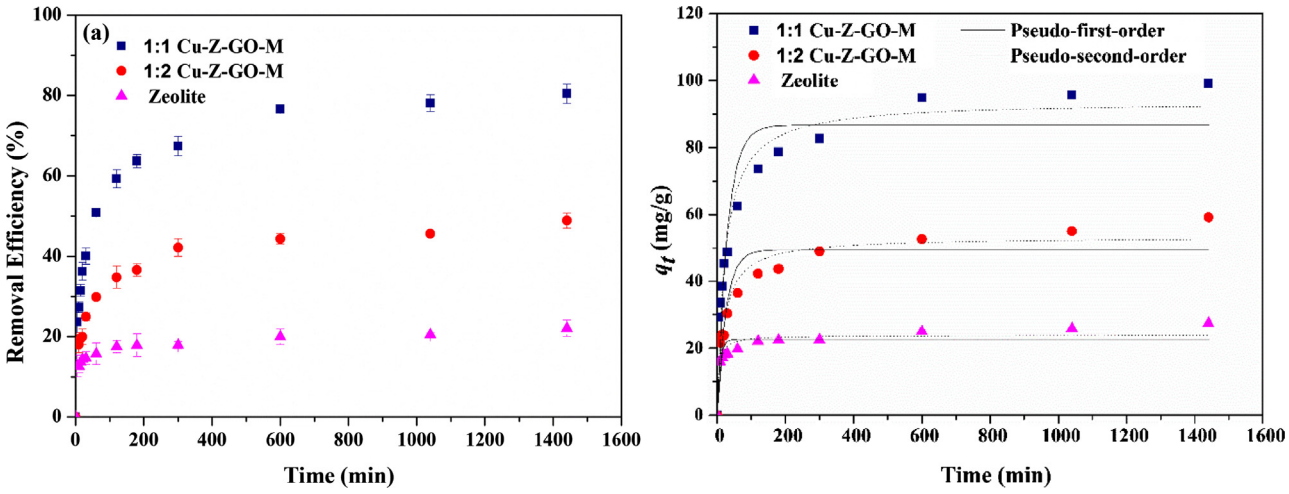


**Fig. 5.** Effect of contact time (a) on the removal efficiency of MB onto absorbents, pseudo-first-order (solid) and pseudo-second-order (dot) non-linear plots (b) of adsorption kinetics for MB onto adsorbents.

**Table 2**
Parameters of kinetic models for the adsorption of MB onto absorbents.

| Models | Pseudo-first-order | | | Pseudo-second-order | | |
|---|---|---|---|---|---|---|
| Parameters | $q_{e,1}$ (mg/g) | $k_1 \times 10$ ($min^{-1}$) | $R^2$ | $q_{e,2}$ (mg/g) | $K_2 \times 10^3$ (g/mg min) | $R^2$ |
| Cu-Z-GO-M (1:1) | 86.635 | 0.337 | 0.895 | 93.781 | 0.472 | 0.963 |
| Cu-Z-GO-M (1:2) | 49.419 | 0.389 | 0.831 | 53.200 | 0.993 | 0.916 |
| Zeolite | 22.701 | 1.288 | 0.805 | 23.931 | 8.725 | 0.907 |

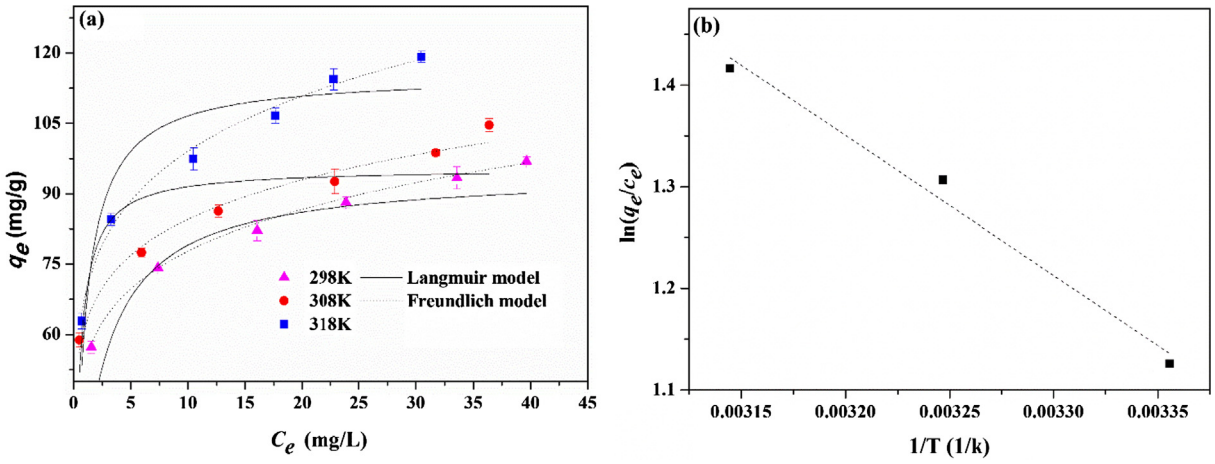


**Fig. 6.** Effect of the temperature on the adsorption of MB onto Cu-Z-GO-M (1:1): Langmuir model (solid) and Freundlich model (dot) non-linear plots of the adsorption isotherm for MB onto Cu-Z-GO-M (1:1) at different temperatures (a), and the thermodynamic analysis (b).

**Table 3**
Constants and correlation coefficients of Langmuir and Freundlich models for MB adsorption onto Cu-Z-GO-M (1:1) at different temperatures.

| T (K) | | 298 K | 308 K | 318 K |
|---|---|---|---|---|
| Langmuir | $q_m$ (mg/g) | 94.481 | 95.369 | 115.322 |
| | $K_L$ (L/mg) | 0.513 | 2.371 | 1.223 |
| | $R^2$ | 0.730 | 0.579 | 0.834 |
| Freundlich | $K_F$ (L/mg) | 54.236 | 61.704 | 68.177 |
| | 1/n | 0.157 | 0.137 | 0.162 |
| | $R^2$ | 0.998 | 0.980 | 0.992 |

**Table 4**
Maximum adsorption capacity ($Q_m$, mg/g) of MB by various absorbents in other reports.

| Absorbents | $Q_m$ (mg/g) | References |
|---|---|---|
| Raw zeolite | 6.1 | [18] |
| Raw kaolin | 13.99 | [53] |
| Graphene oxide | 193.902 | [28] |
| Magnetic multi-wall carbon nanotube | 15.87 | [35] |
| MOF-235 | 187 | [54] |
| 1:1 Cu-Z-GO-M | 94.481 | In this study |

### 3.2.4. Effect of the ionic strength

The ionic strength of solution is another key factor associated with the removal efficiency of MB [59]. In our work, the effect of ionic strength was conducted with NaCl concentrations of 0, 0.01, 0.05, 0.1, 0.2, and 0.5 M in the adsorption systems containing 40 mg/L of MB and 10 mg of absorbent. Fig. 7 displays that the removal efficiency of MB by Cu-Z-GO-M absorbent changes little with the increasing concentration of NaCl. Whereas, the presence of NaCl has a significant effect on MB removal by raw zeolite. This phenomenon may be caused by two reasons: on one hand, the existence of NaCl might screen the surface charges which could suppress the adsorption reaction owing to competitive adsorption, on the other hand it can also enhance the adsorption behavior between MB and three different absorbents by dissociating MB to $MB^+$ [60,61]. The results indicated that the surface charges also played a primary role in the absorption process especially when the absorbent was raw zeolite.

**Table 5**
Thermodynamic analysis data for the adsorption of MB onto Cu-Z-GO-M (1:1).

| T (K) | $lnk^0$ | $\Delta G^0$ (KJ/mol) | $\Delta S^0$ (J/K mol) | $\Delta H^0$ (KJ/mol) | $R^2$ |
|---|---|---|---|---|---|
| 298 K | 1.126 | −2.789 | 5.765 | −1.379 | 0.970 |
| 308 K | 1.307 | −3.237 | | | |
| 318 K | 1.416 | −3.509 | | | |

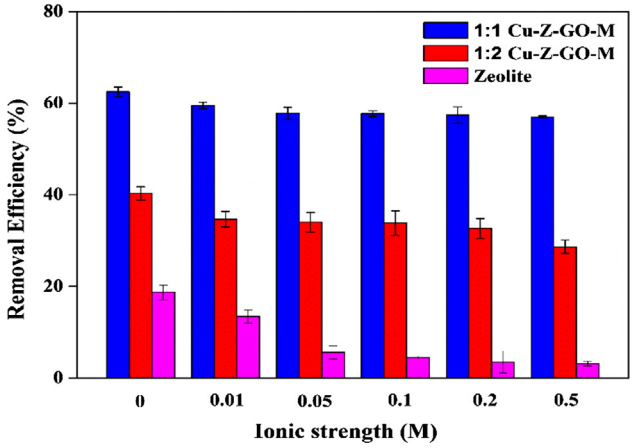


**Fig. 7.** Effect of ionic strength on the removal efficiency of MB adsorption onto absorbents.

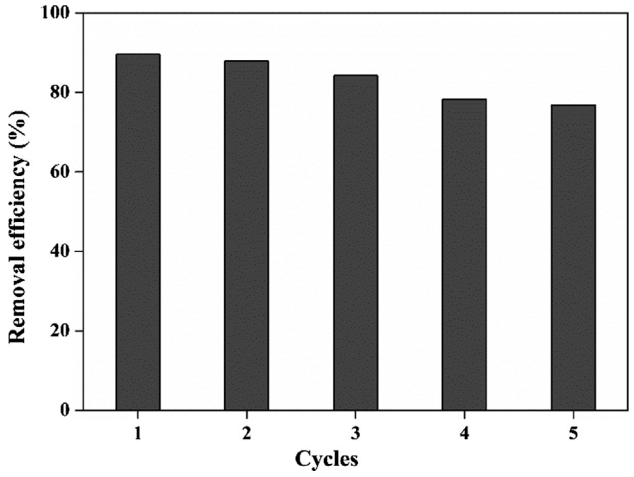


**Fig. 8.** Removal efficiency of MB onto Cu-Z-GO-M (1:1) in five cycles.

### 3.3. Desorption and reusability evaluation

Reusability is another vital factor to assess the application performance of the adsorbent [62]. In this study, Cu-Z-GO-M (1:1), was regarded as the model absorbent due to its highest removal efficiency of dye. Additionally, 0.1 mol/L HCl was chosen as the strippant in this work to realize the release of the MB from the saturated absorbent [63]. Five cycles were applied to verify the stability and reusability of the material. The related results are displayed in Fig. 8. As the regeneration cycles increased, the removal efficiency of MB onto Cu-Z-GO-M decreased (from 89.59% to 76.86%), possibly due to the decline in surface area, the blockage of aperture, and the decrease of active sites available [64]. Although the adsorption decreased, the reduction trend of removal efficiency was not large, which indicated that the reusability of absorbent (Cu-Z-GO-M) was relatively excellent.

## 4. Conclusions

Based on the previously published works [18–20,28–30], this work demonstrated that the magnetic GO modified zeolite samples could be synthesized to facilitate surface characterizations and adsorption capacity towards MB. The introduction of GO to zeolite could enhance the removal ability of MB comparing with zeolite undecorated, which was attributed to the incremental surface area and active sites. The adsorption is better described by pseudo-second-order kinetic and Freundlich isotherm model. A higher temperature and pH are more favorable to MB adsorption. Thermodynamic parameters depicted that the reaction was a spontaneous and endothermic process. After five reused cycles, the removal efficiency of MB onto Cu-Z-GO-M (1:1) was still at a high level (76.86%). This work provided a facial method combined GO and zeolite together to improve the application as well as the adsorption ability of zeolite as the absorbent. Besides, the new findings could not only help us understand how the factors influence the adsorption behavior of MB onto Cu-Z-GO-M, but also prove potential application of Cu-Z-GO-M to solve the dye pollution in the environment.

## Acknowledgements

This study was financially supported by the National Natural Science Foundation of China (51579099, 51521006 and 51879105), Innovative Research Team in University (IRT-13R17), and the Hunan Provincial Innovation Foundation for Postgraduate (CX2016B134).

## References

[1] Y. Xiong, P.J. Strunk, H. Xia, X. Zhu, H.T. Karlsson, Treatment of dye wastewater containing acid orange II using a cell with three-phase three-dimensional electrode, Water Res. 35 (17) (2001) 4226–4230.
[2] Y. Wang, Y. Zhu, Y. Hu, G. Zeng, Y. Zhang, C. Zhang, C. Feng, How to construct DNA hydrogels for environmental applications: advanced water treatment and environmental analysis, Small 14 (17) (2018) 1703305.
[3] L. Zhang, J. Zhang, G. Zeng, H. Dong, Y. Chen, C. Huang, Y. Zhu, R. Xu, Y. Cheng, K. Hou, Multivariate relationships between microbial communities and environmental variables during co-composting of sewage sludge and agricultural waste in the presence of PVP-AgNPs, Bioresour. Technol. 261 (2018) 10–18.
[4] R. Pandimurugan, S. Thambidurai, Synthesis of seaweed-ZnO-PANI hybrid composite for adsorption of methylene blue dye, J. Environ. Chem. Eng. 4 (1) (2016) 1332–1347.
[5] H. Wang, H. Gao, M. Chen, X. Xu, X. Wang, C. Pan, J. Gao, Microwave-assisted synthesis of reduced graphene oxide/titania nanocomposites as an adsorbent for methylene blue adsorption, Appl. Surf. Sci. 360 (2016) 840–848.
[6] M.-X. Zhu, L. Lee, H.-H. Wang, Z. Wang, Removal of an anionic dye by adsorption/precipitation processes using alkaline white mud, J. Hazard. Mater. 149 (3) (2007) 735–741.
[7] H. Yi, D. Huang, G. Zeng, C. Lai, L. Qin, M. Cheng, S. Ye, B. Song, X. Ren, X. Guo, Selective prepared carbon nanomaterials for advanced photocatalytic application in environmental pollutant treatment and hydrogen production, Appl. Catal. B: Environ. (2018).
[8] D. Xu, B. Cheng, S. Cao, J. Yu, Enhanced photocatalytic activity and stability of Z-scheme $Ag_2CrO_4$-GO composite photocatalysts for organic pollutant degradation, Appl. Catal. B 164 (2015) 380–388.
[9] Y. Yang, C. Zhang, C. Lai, G. Zeng, D. Huang, M. Cheng, J. Wang, F. Chen, C. Zhou, W. Xiong, BiOX (X= Cl, Br, I) photocatalytic nanomaterials: applications for fuels and environmental management, Adv. Colloid Interface Sci. (2018).
[10] D.R. Manenti, A.N. Módenes, P.A. Soares, F.R. Espinoza-Quiñones, R.A. Boaventura, R. Bergamasco, V.J. Vilar, Assessment of a multistage system based on electrocoagulation, solar photo-Fenton and biological oxidation processes for real textile wastewater treatment, Chem. Eng. J. 252 (2014) 120–130.
[11] X. Ren, G. Zeng, L. Tang, J. Wang, J. Wan, H. Feng, B. Song, C. Huang, X. Tang, Effect of exogenous carbonaceous materials on the bioavailability of organic pollutants and their ecological risks, Soil Biol. Biochem. 116 (2018) 70–81.
[12] S. Fan, J. Tang, Y. Wang, H. Li, H. Zhang, J. Tang, Z. Wang, X. Li, Biochar prepared from co-pyrolysis of municipal sewage sludge and tea waste for the adsorption of methylene blue from aqueous solutions: kinetics, isotherm, thermodynamic and mechanism, J. Mol. Liq. 220 (2016) 432–441.
[13] K. He, Z. Zeng, A. Chen, G. Zeng, R. Xiao, P. Xu, Z. Huang, J. Shi, L. Hu, G. Chen, Advancement of Ag–graphene based nanocomposites: an overview of synthesis and its applications, Small 14 (32) (2018) 1800871.
[14] Q. Li, Y. Li, X. Ma, Q. Du, K. Sui, D. Wang, C. Wang, H. Li, Y. Xia, Filtration and adsorption properties of porous calcium alginate membrane for methylene blue removal from water, Chem. Eng. J. 316 (2017) 623–630.
[15] G. Crini, Non-conventional low-cost adsorbents for dye removal: a review, Bioresour. Technol. 97 (9) (2006) 1061–1085.
[16] Z. Huang, G. Chen, G. Zeng, A. Chen, Y. Zuo, Z. Guo, Q. Tan, Z. Song, Q. Niu, Polyvinyl alcohol-immobilized Phanerochaete chrysosporium and its application in the bioremediation of composite-polluted wastewater, J. Hazard. Mater. 289 (2015) 174–183.

[17] S. Wang, Z. Zhu, Characterisation and environmental application of an Australian natural zeolite for basic dye removal from aqueous solution, J. Hazard. Mater. 136 (3) (2006) 946–952.
[18] X. Jin, M.-Q. Jiang, X.-Q. Shan, Z.-G. Pei, Z. Chen, Adsorption of methylene blue and orange II onto unmodified and surfactant-modified zeolite, J. Colloid Interface Sci. 328 (2) (2008) 243–247.
[19] R. Han, J. Zhang, P. Han, Y. Wang, Z. Zhao, M. Tang, Study of equilibrium, kinetic and thermodynamic parameters about methylene blue adsorption onto natural zeolite, Chem. Eng. J. 145 (3) (2009) 496–504.
[20] E. Alver, A.Ü. Metin, Anionic dye removal from aqueous solutions using modified zeolite: adsorption kinetics and isotherm studies, Chem. Eng. J. 200 (2012) 59–67.
[21] K. Haubner, J. Murawski, P. Olk, L.M. Eng, C. Ziegler, B. Adolphi, E. Jaehne, The route to functional graphene oxide, ChemPhysChem 11 (10) (2010) 2131–2139.
[22] Z. Huang, Z. Zeng, A. Chen, G. Zeng, R. Xiao, P. Xu, K. He, Z. Song, L. Hu, M. Peng, Differential behaviors of silver nanoparticles and silver ions towards cysteine: bioremediation and toxicity to *Phanerochaete chrysosporium*, Chemosphere 203 (2018) 199–208.
[23] K. He, G. Chen, G. Zeng, A. Chen, Z. Huang, J. Shi, T. Huang, M. Peng, L. Hu, Three-dimensional graphene supported catalysts for organic dyes degradation, Appl. Catal. B: Environ. (2018).
[24] C.J. Madadrang, H.Y. Kim, G. Gao, N. Wang, J. Zhu, H. Feng, M. Gorring, M.L. Kasner, S. Hou, Adsorption behavior of EDTA-graphene oxide for Pb (II) removal, ACS Appl. Mater. Interfaces 4 (3) (2012) 1186–1193.
[25] Z. Huang, P. Xu, G. Chen, G. Zeng, A. Chen, Z. Song, K. He, L. Yuan, H. Li, L. Hu, Silver ion-enhanced particle-specific cytotoxicity of silver nanoparticles and effect on the production of extracellular secretions of *Phanerochaete chrysosporium*, Chemosphere 196 (2018) 575–584.
[26] Z. Huang, K. He, Z. Song, G. Zeng, A. Chen, L. Yuan, H. Li, L. Hu, Z. Guo, G. Chen, Antioxidative response of *Phanerochaete chrysosporium* against silver nanoparticle-induced toxicity and its potential mechanism, Chemosphere 211 (2018) 573–583.
[27] Z. Huang, G. Chen, G. Zeng, Z. Guo, K. He, L. Hu, J. Wu, L. Zhang, Y. Zhu, Z. Song, Toxicity mechanisms and synergies of silver nanoparticles in 2, 4-dichlorophenol degradation by *Phanerochaete chrysosporium*, J. Hazard. Mater. 321 (2017) 37–46.
[28] K. He, G. Chen, G. Zeng, A. Chen, Z. Huang, J. Shi, M. Peng, T. Huang, L. Hu, Enhanced removal performance for methylene blue by kaolin with graphene oxide modification, J. Taiwan Inst. Chem. Eng. (2018).
[29] Y. Yu, B.N. Murthy, J.G. Shapter, K.T. Constantopoulos, N.H. Voelcker, A.V. Ellis, Benzene carboxylic acid derivatized graphene oxide nanosheets on natural zeolites as effective adsorbents for cationic dye removal, J. Hazard. Mater. 260 (2013) 330–338.
[30] M. Khatamian, N. Khodakarampoor, M. Saket-Oskoui, Efficient removal of arsenic using graphene-zeolite based composites, J. Colloid Interface Sci. 498 (2017) 433–441.
[31] P.T.L. Huong, V.N. Phan, T.Q. Huy, M.H. Nam, V.D. Lam, A.-T. Le, Application of graphene oxide-$MnFe_2O_4$ magnetic nanohybrids as magnetically separable adsorbent for highly efficient removal of arsenic from water, J. Electron. Mater. 45 (5) (2016) 2372–2380.
[32] P. Xu, G.M. Zeng, D.L. Huang, C.L. Feng, S. Hu, M.H. Zhao, C. Lai, Z. Wei, C. Huang, G.X. Xie, Use of iron oxide nanomaterials in wastewater treatment: a review, Sci. Total Environ. 424 (2012) 1–10.
[33] Y.-G. Liu, X.-J. Hu, H. Wang, A.-W. Chen, S.-M. Liu, Y.-M. Guo, Y. He, X. Hu, J. Li, S.-H. Liu, Photoreduction of Cr (VI) from acidic aqueous solution using $TiO_2$-impregnated glutaraldehyde-crosslinked alginate beads and the effects of Fe (III) ions, Chem. Eng. J. 226 (2013) 131–138.
[34] X. Tang, G. Zeng, C. Fan, M. Zhou, L. Tang, J. Zhu, J. Wan, D. Huang, M. Chen, P. Xu, Chromosomal expression of CadR on Pseudomonas aeruginosa for the removal of Cd (II) from aqueous solutions, Sci. Total Environ. 636 (2018) 1355–1361.
[35] J.-L. Gong, B. Wang, G.-M. Zeng, C.-P. Yang, C.-G. Niu, Q.-Y. Niu, W.-J. Zhou, Y. Liang, Removal of cationic dyes from aqueous solution using magnetic multi-wall carbon nanotube nanocomposite as adsorbent, J. Hazard. Mater. 164 (2–3) (2009) 1517–1522.
[36] Y. Yang, Z. Zeng, C. Zhang, D. Huang, G. Zeng, R. Xiao, C. Lai, C. Zhou, H. Guo, W. Xue, Construction of iodine vacancy-rich BiOI/Ag@ AgI Z-scheme heterojunction photocatalysts for visible-light-driven tetracycline degradation: transformation pathways and mechanism insight, Chem. Eng. J. 349 (2018) 808–821.
[37] S. Kumar, R.R. Nair, P.B. Pillai, S.N. Gupta, M. Iyengar, A. Sood, Graphene oxide–MnFe2O4 magnetic nanohybrids for efficient removal of lead and arsenic from water, ACS Appl. Mater. Interfaces 6 (20) (2014) 17426–17436.
[38] M. Khatamian, N. Khodakarampoor, M.S. Oskoui, N. Kazemian, Synthesis and characterization of RGO/zeolite composites for the removal of arsenic from contaminated water, RSC Adv. 5 (45) (2015) 35352–35360.
[39] M. Liu, C. Chen, J. Hu, X. Wu, X. Wang, Synthesis of magnetite/graphene oxide composite and application for cobalt (II) removal, J. Phys. Chem. C 115 (51) (2011) 25234–25240.
[40] A. Ye, W. Fan, Q. Zhang, W. Deng, Y. Wang, CdS–graphene and CdS–CNT nanocomposites as visible-light photocatalysts for hydrogen evolution and organic dye degradation, Catal. Sci. Technol. 2 (5) (2012) 969–978.
[41] H. Liu, S. Ji, Y. Zheng, M. Li, H. Yang, Modified solvothermal synthesis of magnetic microspheres with multifunctional surfactant cetyltrimethyl ammonium bromide and directly coated mesoporous shell, Powder Technol. 246 (2013) 520–529.
[42] C. Cao, L. Xiao, C. Chen, X. Shi, Q. Cao, L. Gao, In situ preparation of magnetic $Fe_3O_4$/chitosan nanoparticles via a novel reduction–precipitation method and their application in adsorption of reactive azo dye, Powder Technol. 260 (2014) 90–97.
[43] V. Chandra, J. Park, Y. Chun, J.W. Lee, I.-C. Hwang, K.S. Kim, Water-dispersible magnetite-reduced graphene oxide composites for arsenic removal, ACS Nano 4 (7) (2010) 3979–3986.
[44] S. Luo, X. Xu, G. Zhou, C. Liu, Y. Tang, Y. Liu, Amino siloxane oligomer-linked graphene oxide as an efficient adsorbent for removal of Pb (II) from wastewater, J. Hazard. Mater. 274 (2014) 145–155.
[45] A. Tehrani-Bagha, H. Nikkar, N. Mahmoodi, M. Markazi, F. Menger, The sorption of cationic dyes onto kaolin: kinetic, isotherm and thermodynamic studies, Desalination 266 (1–3) (2011) 274–280.
[46] Z. Yin, Y. Liu, S. Liu, L. Jiang, X. Tan, G. Zeng, M. Li, S. Liu, S. Tian, Y. Fang, Activated magnetic biochar by one-step synthesis: enhanced adsorption and coadsorption for 17β-estradiol and copper, Sci. Total Environ. 639 (2018) 1530–1542.
[47] L. Jiang, Y. Liu, G. Zeng, S. Liu, X. Hu, L. Zhou, X. Tan, N. Liu, M. Li, J. Wen, Adsorption of estrogen contaminants (17β-estradiol and 17α-ethynylestradiol) by graphene nanosheets from water: effects of graphene characteristics and solution chemistry, Chem. Eng. J. 339 (2018) 296–302.
[48] W. Zeng, Y.-G. Liu, X.-J. Hu, S.-B. Liu, G.-M. Zeng, B.-H. Zheng, L.-H. Jiang, F.-Y. Guo, Y. Ding, Y. Xu, Decontamination of methylene blue from aqueous solution by magnetic chitosan lignosulfonate grafted with graphene oxide: effects of environmental conditions and surfactant, RSC Adv. 6 (23) (2016) 19298–19307.
[49] G. Ramesha, A.V. Kumara, H. Muralidhara, S. Sampath, Graphene and graphene oxide as effective adsorbents toward anionic and cationic dyes, J. Colloid Interface Sci. 361 (1) (2011) 270–277.
[50] B.K. Nandi, A. Goswami, M.K. Purkait, Adsorption characteristics of brilliant green dye on kaolin, J. Hazard. Mater. 161 (1) (2009) 387–395.
[51] M. Rauf, S. Bukallah, F. Hamour, A. Nasir, Adsorption of dyes from aqueous solutions onto sand and their kinetic behavior, Chem. Eng. J. 137 (2) (2008) 238–243.
[52] W. Xiong, Z. Zeng, X. Li, G. Zeng, R. Xiao, Z. Yang, Y. Zhou, C. Zhang, M. Cheng, L. Hu, Multi-walled carbon nanotube/amino-functionalized MIL-53 (Fe) composites: remarkable adsorptive removal of antibiotics from aqueous solutions, Chemosphere 210 (2018) 1061–1069.
[53] D. Ghosh, K.G. Bhattacharyya, Adsorption of methylene blue on kaolinite, Appl. Clay Sci. 20 (6) (2002) 295–300.
[54] E. Haque, J.W. Jun, S.H. Jhung, Adsorptive removal of methyl orange and methylene blue from aqueous solution with a metal-organic framework material, iron terephthalate (MOF-235), J. Hazard. Mater. 185 (1) (2011) 507–511.
[55] L. Fan, C. Luo, X. Li, F. Lu, H. Qiu, M. Sun, Fabrication of novel magnetic chitosan grafted with graphene oxide to enhance adsorption properties for methyl blue, J. Hazard. Mater. 215 (2012) 272–279.
[56] C. Zhou, C. Lai, C. Zhang, G. Zeng, D. Huang, M. Cheng, L. Hu, W. Xiong, M. Chen, J. Wang, Semiconductor/boron nitride composites: synthesis, properties, and photocatalysis applications, Appl. Catal. B (2018).
[57] L. Qin, G. Zeng, C. Lai, D. Huang, P. Xu, C. Zhang, M. Cheng, X. Liu, S. Liu, B. Li, "Gold rush" in modern science: fabrication strategies and typical advanced applications of gold nanoparticles in sensing, Coord. Chem. Rev. 359 (2018) 1–31.
[58] S. Ye, G. Zeng, H. Wu, C. Zhang, J. Liang, J. Dai, Z. Liu, W. Xiong, J. Wan, P. Xu, Co-occurrence and interactions of pollutants, and their impacts on soil remediation—a review, Critic. Rev. Environ. Sci. Technol. 47 (16) (2017) 1528–1553.
[59] B. Meroufel, O. Benali, M. Benyahia, Y. Benmoussa, M. Zenasni, Adsorptive removal of anionic dye from aqueous solutions by Algerian kaolin: characteristics, isotherm, kinetic and thermodynamic studies, J. Mater. Environ. Sci 4 (3) (2013) 482–491.
[60] B. Nandi, A. Goswami, M. Purkait, Removal of cationic dyes from aqueous solutions by kaolin: kinetic and equilibrium studies, Appl. Clay Sci. 42 (3–4) (2009) 583–590.
[61] X. Ren, G. Zeng, L. Tang, J. Wang, J. Wan, Y. Liu, J. Yu, H. Yi, S. Ye, R. Deng, Sorption, transport and biodegradation–an insight into bioavailability of persistent organic pollutants in soil, Sci. Total Environ. 610 (2018) 1154–1163.
[62] M. Peng, G. Chen, G. Zeng, A. Chen, K. He, Z. Huang, L. Hu, J. Shi, H. Li, L. Yuan, Superhydrophobic kaolinite modified graphene oxide-melamine sponge with excellent properties for oil-water separation, Appl. Clay Sci. 163 (2018) 63–71.
[63] S. Ye, G. Zeng, H. Wu, C. Zhang, J. Dai, J. Liang, J. Yu, X. Ren, H. Yi, M. Cheng, Biological technologies for the remediation of co-contaminated soil, Crit. Rev. Biotechnol. 37 (8) (2017) 1062–1076.
[64] M. Auta, B. Hameed, Chitosan–clay composite as highly effective and low-cost adsorbent for batch and fixed-bed adsorption of methylene blue, Chem. Eng. J. 237 (2014) 352–361.